17th World Conference on Earthquake Engineering, 17WCEE
Sendai, Japan - September 13th to 18th 2020

QUANTIFICATION OF SURFACE WAVES IN ALLUVIAL BASIN: SIMULATIONS FOR CANONICAL AND REALISTIC CASES

J.F. Semblat[(1)], K. Meza-Fajardo[(2)], S. Chaillat[(3)], C. Varone[(4)], L. Lenti[(5)], S.Touhami[(6)]

[(1)] *IMSIA UMR9219, CNRS-EDF-CEA-ENSTA Paris, Institut Polytechnique de Paris, Palaiseau, France, jean-francois.semblat@ensta-paris.fr*
[(2)] *Risk and Prevention Division, BRGM, Orléans, France*
[(3)] *Poems UMR 7231, CNRS-INRIA-ENSTA Paris, Institut Polytechnique de Paris, Palaiseau, France*
[(4)] *Dept of Geotechnical Eng., Université Gustave Eiffel, Champs-sur-Marne, France*
[(5)] *ESITC-Paris, France*
[(6)] *Poems UMR 7231, CNRS-INRIA-ENSTA Paris, Institut Polytechnique de Paris, Palaiseau, France*

Abstract

Seismic waves propagating in alluvial deposits may generate surface waves due to lateral heterogeneities. Such basin edge generated surface waves strengthen the amplification process and lead to long period ground motions. These long period excitations may be detrimental for tall or large structures.

This paper focuses on the quantification of basin edge generated surface waves by time-frequency analysis. Numerical simulations for canonical and realistic configurations lead to various seismograms involving a significant amount of surface waves. The normalized inner product proposed by Meza-Fajardo et al. (2015) allows to identify and quantify the contribution of surface waves in the total computed ground motion. For canonical basins, the influence of the basin edge slope and of the basin/bedrock impedance contrast on the amount of surface waves is characterized. For an actual configuration in the city of Rome, the highly heterogeneous deposit leads to strong surface waves of various origins: basin edge generated wavefield, sub-basin effects for non-smooth deposit geometries, local strong heterogeneities. It is thus very important to identify these various contributions in order to characterize the basin effects and the long period seismic ground motions (azimuth, amplitude, time window).

This work is part of the Modulate research project funded by French National Research Agency (ANR).

Keywords: site effects, surface waves, numerical modeling, time-frequency analysis.

1. Introduction

The amplification of seismic waves in alluvial deposits is strongly influenced by the geometry and mechanical properties of the surficial layers. The amplification process can significantly differ between the 1D (horizontal layering) and the 2D/3D cases because of focusing effects and waves generated at basin edges, (e.g., Paolucci 1999). Some analytical and numerical results have been already derived by various authors for the response of basins with simple geometries to incident waves. Bard and Bouchon (1985) studied rectangular and sine-shaped soft layers embedded in a rigid half space considering incident plane SH-waves. The propagation of plane vertical SH-waves in 2D cylindrical basins was analyzed by Semblat et al. (2010) using the Boundary Element Method in the frequency domain. Rodriguez-Zuñiga et al. (2005) studied the case of a 3D cylindrical basin having a rectangular vertical cross-section and found a large difference between the 2D and 3D response at the center of the basin. In the works of Bard and Bouchon (1985) and Jiang and Kuribayashi (1988), it was reported that the fundamental frequencies of the basins only depend on the aspect ratio and the 1D fundamental frequency at the center of the valley. The 3D wave diffraction by a semi-spherical canyon has been also studied (Kim and Papageorgiou 1993; Yokoi 2003; Chaillat et al. 2008) and 3D wave amplification due to surface heterogeneities has also been quantified (Sánchez-Sesma and Luzón, 1995; Komatitsch and Vilottte 1998; Drawinski 2003; Moczo et al. 2002; Chaillat et al. 2009). Smerzini et al. (2011) made comparisons of 3D, 2D and 1D amplification using the Spectral Element Method with a 3D model of the Gubbio plain in Italy. Olsen et al. (2000) found differences among 3D/2.5D/1D amplification and duration with a 3D finite difference model of the Upper Borrego Valley, California. The 2D amplification features may be interpreted through 2D/1D amplification factors with respect to the case of a horizontal layer (Chavez-Garcia and Faccioli 2000, Makra et al. 2005). The assessment of the effect of surface waves in different 2D and 3D configurations is the main goal of this paper.

2. 2D aggravation due to surface waves

2.1 Simple configurations

We first consider various 2D elliptical basins for plane SH-waves (Semblat et al., 2010). Their horizontal shape ratios, $\kappa_h=L/H$, are chosen as κ_h=0.5; 1; 2; 3; 4; 5 and 6 (L is the half-width of the basin and H its depth kept constant H=25m). Different velocity ratios are also chosen: χ=2–8. From all these models, the maximum motion amplification and the related frequency are computed. The results are plotted in Fig. 1 as an abacus: solid lines correspond to fixed shape ratios κ_h and dotted lines to constant velocity ratios χ. The main conclusions are the following:

- For a constant velocity ratio and shape ratios larger than 1, the maximum amplification and the related frequency decrease when increasing the shape ratio; the results then become closer to the 1D case.
- For narrow basins (small shape ratios), the 2D results are far from the 1D analysis (strong 2D effects due to the generation of surface waves).
- For a constant shape ratio, when the velocity ratio increases, the maximum amplification increases and the related frequency decreases.

From Fig. 1, it is thus possible to estimate the maximum ground motion amplification and the related frequency for various types of 2D alluvial basins. Our numerical results for an elliptical basin were compared to Bard and Bouchon's results (1985) for sinusoidal basins. Our frequencies of maximum amplification have similar variations with respect to the shape ratio. 2D effects are found to be strong for narrow basins due to surface waves whereas large basins lead to amplification levels close to the 1D case.

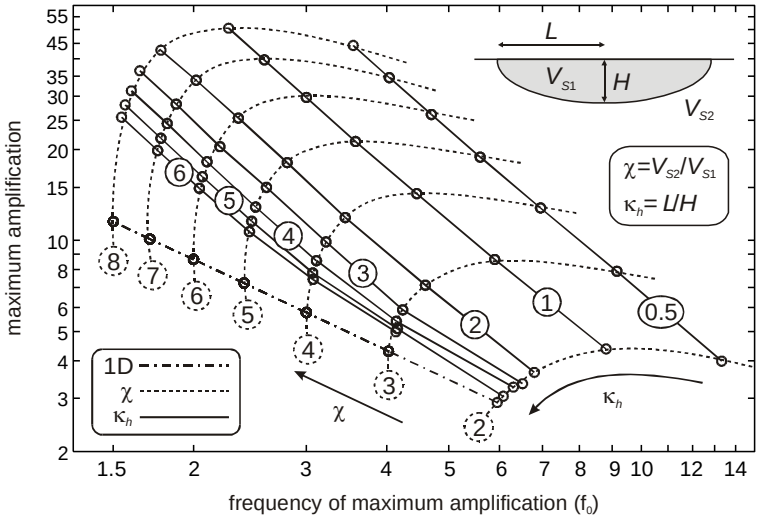

Fig. 1 – Maximum amplification and related frequencies (in Hz) for variable shape ratios κ_h and velocity ratios χ. Here the symbol *L* has been used instead of *R* for the radius of the basin (Semblat *et al*., 2010).

2.2 Actual basin geometries

The Volvi test site in Greece has been studied for many years. Figure 2 depicts a 2D cross-section of the main basin. This detail geotechnical model involves six soil layers above an elastic bedrock; the Young modulus for layer 1 is 180 MPa and that in the bedrock is 4200 MPa (Semblat et al., 2005). The main goal here is to investigate the influence of the knowledge of the local geology on site effects computations. The 2D basin effects will be investigated in terms of surface wave generation.

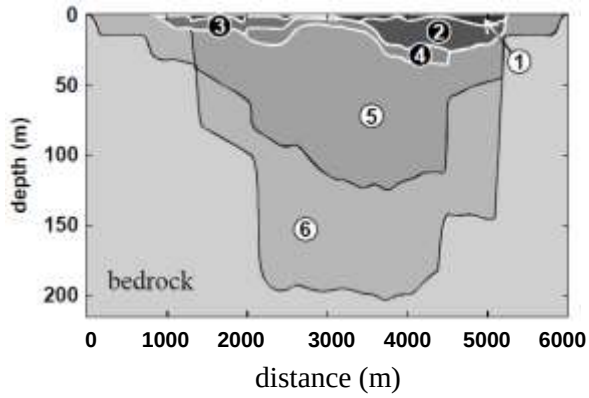

Fig. 2 – Detailed 2D geotechnical models of the Volvi basin (Semblat et al., 2005).

To fully understand the influence of the basin model description (i.e. both vertical and horizontal heterogeneities), we will compute the time domain responses at the free surface. For the detailed geotechnical model, we consider an upward propagating SH-wave described by a Ricker signal whose spectrum is centered at 1 Hz. From frequency domain Boundary Elements simulations (Semblat et al. 2005), we compute the time domain seismic waves along the free surface. In Fig. 3 are displayed the time domain results along the basin for both types of models.

From the time domain solutions of Fig. 3, the 2D amplification process appears clearly. The effect of lateral heterogeneities (basin effects) is obvious since wave reflections on basin edges occur. The amplification of the first arrivals also shows the influence of the velocity contrast in the central (deepest) part of the basin. Seismic wave amplification in the simplified Volvi basin is then influenced by both vertical (soil layering) and lateral (basin effects) heterogeneities.

These basin effects are mainly due to surface wave generation at the basin edges. The soil layering being described precisely, the incident Ricker wavelet is combined with reflected and refracted waves to give a more complex wave field (Fig. 3). It is especially the case on both left and right sides of the deepest part of the basin. It is possibly due to the combination of vertical and lateral heterogeneities influences. Since, the velocity contrasts are described precisely in this detailed model, the lateral wave propagation in each layer is made easier and surface wave generation at the basin edges strengthens the global amplification process. Concerning the signal duration, it is significantly increased showing once more the combined influence of basin effect and soil layering.

The influence of the soil layering of the basin on the amplification process as well as on the signals duration raises the need for a very detailed knowledge of the soil properties and layers geometry. This is a key point to have reliable prediction of surface seismic motion in alluvial deposits.

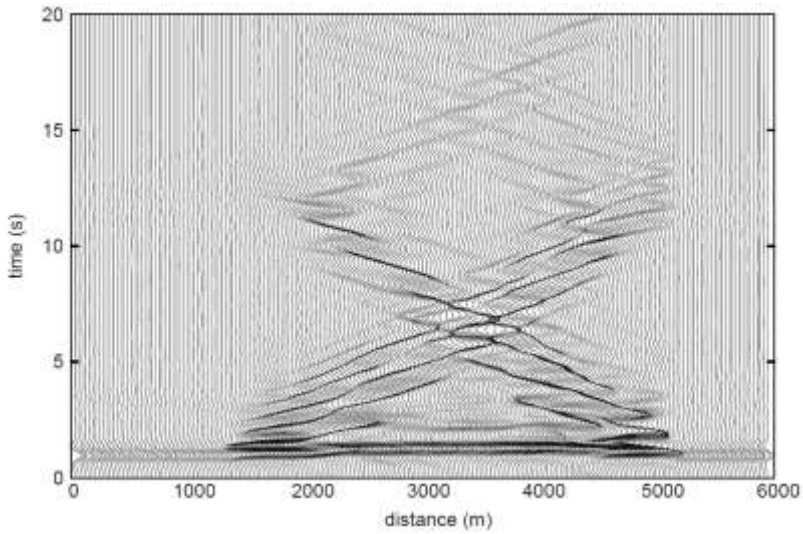

Fig. 3 – Time domain signals for the complete Volvi basin models under a 1 Hz Ricker excitation (Semblat et al., 2005).

3. 3D aggravation due to surface waves

The 3D amplification of seismic waves is modeled through the Fast Multipole Method (FMM). This formulation of the Boundary Element Method (BEM) allows the acceleration of iterative solvers for the global linear system of equations. The application of the Fast Multipole Boundary Element Method (FMBEM) is beneficial in problems of elastic wave propagation involving strong velocity gradients or 3D unbounded domains since large BEM meshes are required (Makra et al. 2005; Chaillat et al. 2008; Chaillat et al. 2009; Delépine & Semblat 2012). Extension of the FMBEM to propagation in weakly dissipative viscoelastic media was carried out by Grasso et al. (2012). In this section, we apply the formulation of the FMBEM for viscoelastic media to study wave amplification phenomena in 3D basins with canonical geometries subjected to incident plane waves. Following the work done by Makra et al. (2005) and Semblat et al. (2010) for canonical or realistic 2D configurations, we identify the fundamental frequencies of the basin, and study the relationships between the amplification level and relevant mechanical parameters such as impedance contrast, aspect ratio and damping.

We compare here the amplification factor for three different 3-D shapes. The elliptical shape has already been described in the previous section (2D case). The second shape we consider corresponds to a super-ellipsoid of fifth degree (instead of 2 for regular ellipsoids).

When the exponent of the super-ellipsoid is 5 the basin geometry is closer to a "box" shape as shown in Figure 4. The third shape we consider in this study is a 3D cosine shape depicted in Fig.4. Note that the total depth of the basin is 1, but the shape is scaled such that its height is only 90% of the total height of a full cosine cycle. We selected this percentage instead of the complete height of the cosine (for which p would be 1) to avoid numerical artifacts at the intersection of the basin boundary and the free surface, which occur when two surfaces intersect with the same tangent.

Considering the "equivalent shape ratio" $\kappa_h^* = l_0/h$ used by Jiang and Kirubashi (1988), where l_0 is the half width over which the depth of the basin is half its maximum value, we can take into account the difference in thickness of the three basin shapes, as shown in Figure 4. We can see in Figure 4 (right) that even though the three shapes have the same aspect ratio ($\kappa_h = R/h$) the cosine shape has the lowest equivalent shape ratio.

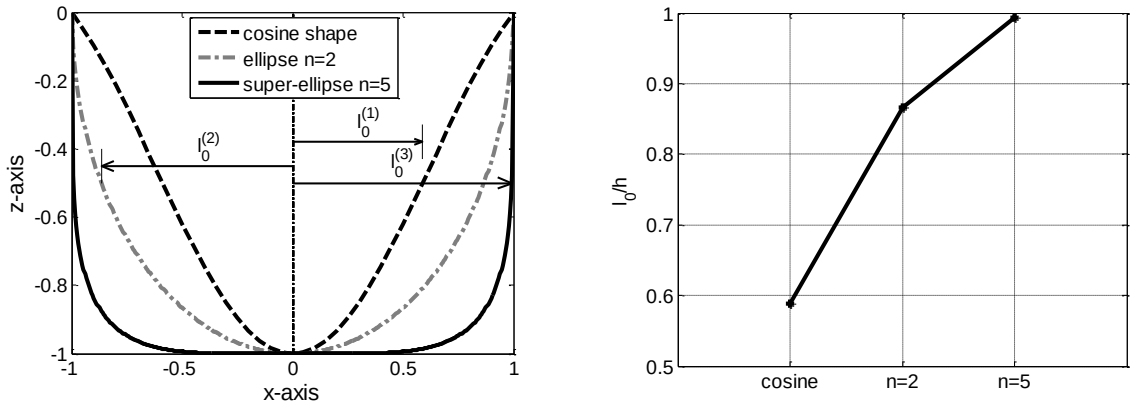

Fig. 4 – Basin shapes considered in the study. Cross section corresponding to the *x-z* plane (left), equivalent shape ratio l_0/h for the three basin shapes for a unitary radius (right).

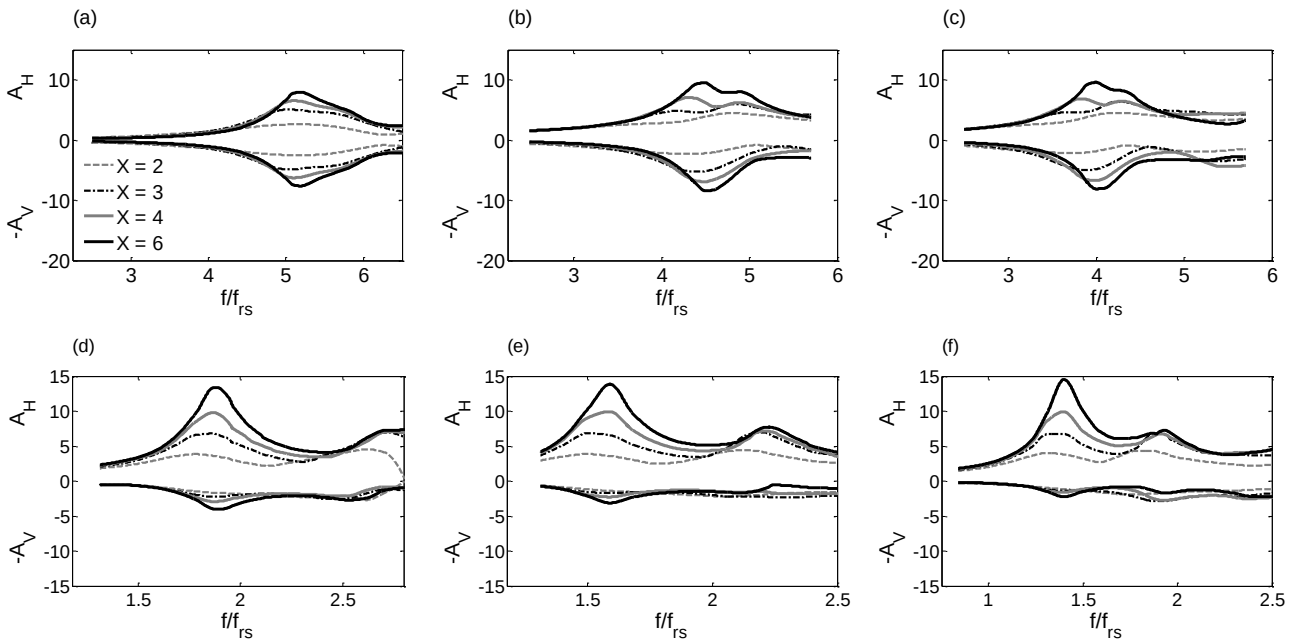

Fig. 5 – Amplification at the top of the 3D basin (5% damping) due to vertically incident *S*-waves with different equivalent shape ratios. (a) R/h=0.5 with cosine shape (b) R/h=0.5 with ellipsoidal shape, n=2 (c) R/h=0.5 with super-ellipsoidal shape, n=5 (d) R/h=2, with cosine shape (e) R/h=2 with ellipsoidal shape, n=2 (f) R/h=2 with super-ellipsoidal shape, n=5.

In Figure 5 we can see the effect of different equivalent shape ratios on the amplification factors for the three different basin shapes, when they are subjected to vertically propagating *S*-waves, for the case of an aspect ratio κ_h=0.5 (Figures 5a-5c) and κ_h=2 (Figures 5e-5f). The amplification level for the ellipsoidal shapes remains almost the same, both for the horizontal and vertical components; however the difference in the exponent *n* leads to different fundamental and dominant frequencies. On the other hand, we can see slightly higher amplification factors for the fundamental frequency in the case of the basin with cosine shape, a result that was expected, since there are strong basin edge effects and there is more trapping of waves due to the lower thickness of the basin. Surface wave generation also appears different between the wide and narrow cases.

4. Quantification of surface waves in alluvial basin

4.1 Seismic response of the Fosso di Vallerano valley (Rome)

Since the basin effects may be very large depending on the basin shape and velocity constrast, it may be useful to assess the amount of surface waves in the total wavefield. To do so, we shall now consider the Fosso di Vallerano valley in the city of Rome (Meza-Fajardo et al., 2019).

The geological cross section AA' is depicted in Fig.6. It is subjected to aseismic excitation in the form of vertically incident plane S waves. Because we are interested in the analysis of Rayleigh waves, we set a peak unitary vertical displacement. The time variation of the input motion is given by a 0th-order Ricker wavelet with frequency content from 0.1 to 15 Hz. To investigate the effects of the valley on the wave field, several recording stations (receivers) are selected along the free surface of the cross sections, as shown in Figure 6.

The results of the simulations for cross section AA' is shown in Figure 6, where displacement histories at the receivers are displayed. Visual inspection of the figures show a later arrival time of the first phases at the center of the basin, a consequence of the lower velocity of propagation in the soft layers. We can also observe how low frequency phases are more distributed in time for the stations at the center of the basin, signaling dispersion as one basin effect. A more detailed account of basin effects is presented in the following section, where a time-frequency processing is applied to the time histories.

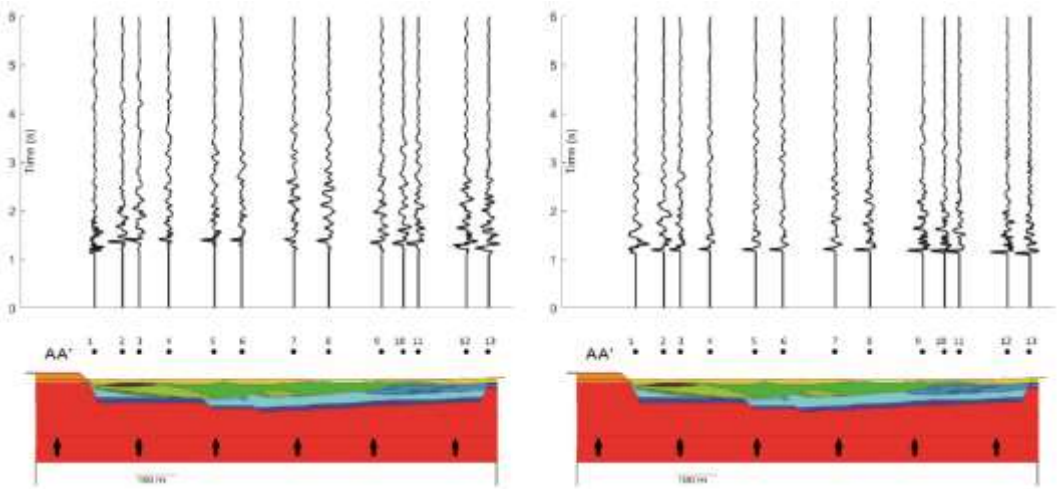

Fig. 6 – Displacement histories for receivers at the free surface of cross sections AA'. Horizontal component (left), Vertical component (right).

4.2 Surface wave quantification for the Fosso di Vallerano valley (Rome)

To quantify the amount of surface waves in the seismic response of the Fosso di Vallerano Valley, The Normalized Inner Product proposed by Meza-Fajardo et al. (2015) is applied. To illustrate the procedure, we show in Figure 7 the time-frequency Stockwell Transforms of the horizontal and vertical components at station 13. We can observe that in the vertical component most of the energy is concentrated before 2 seconds, whereas in the horizontal component dominant frequencies are more distributed in time.

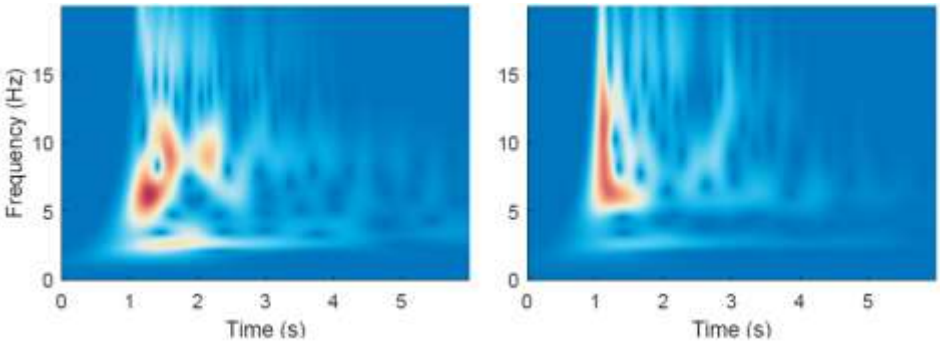

Fig. 7 – Stockwell Transforms of displacement components at station 13 of cross section AA'. Horizontal component (left), Vertical component (right).

From the Stockwell transform, the Normalized Inner Product is computed and significant time-frequency amplitudes are retained to account for surface waves (Meza-Fajardo et al., 2015). The time histories of the two components of the extracted Rayleigh waves are shown in Figure 8, for all the other stations in cross section AA'. We can observe that the Rayleigh waves with higher amplitudes are found in those stations close to the basin edges. As shown in Meza-Fajardo et al. (2019), we may also assess the influence of sub-basins in another profile of the Fosso di Vallerano valley.

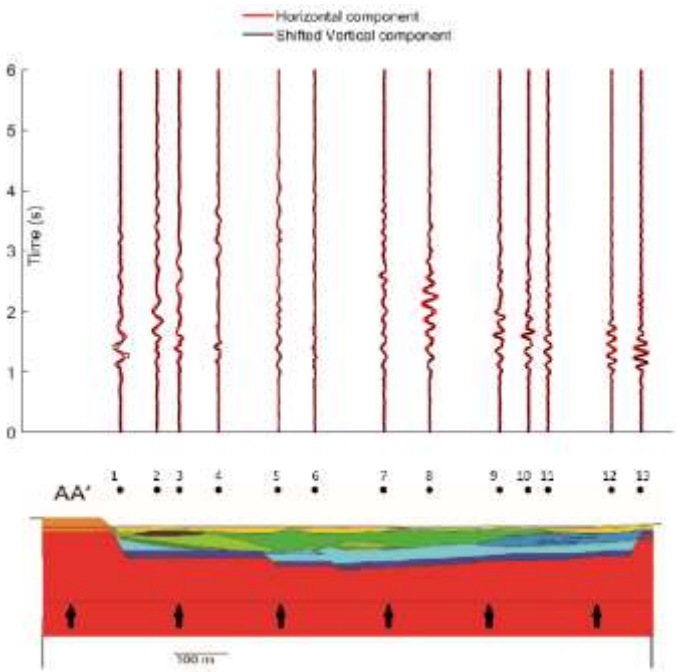

Fig. 8 – Horizontal and vertical components of extracted Rayleigh waves at stations on cross section AA'. The vertical component has a -π/2 shift.

However, the edge-generated Rayleigh waves do not seem to preserve their amplitude in the more internal stations of the basins, probably due to inelastic attenuation and the interference of all waves diffracted by the complex soil layering. At station 8 of section AA' (Figure 8), we can observe the presence of a Rayleigh wave with high amplitude and long duration, of lower frequency. The concentration of energy giving rise to this wave might be possible due to the very thick soil deposits (layers 4 and 11) below the station. On the other hand, we could claim that there are no extracted surface waves at station 6 as there are no clear extracted wavetrains, and that the motion shown in Figure 8 at this station is simply numerical noise.

5. Conclusions

The amplification of seismic waves is strengthened in 2D and 3D alluvial deposits due to basin effects. The main contribution is due to surface wave generation at the basin edges (or even internal sub-basins). As shown by 2D and 3D canonical configurations, it is possible to assess the 2D and 3D effects for simple basin shapes. For more general cases (Volvi, Rome), the basin edge generated surface waves can be computed for simple input motions. Furthermore the Normalized Inner Spectrum proposed by Meza-Fajardo et al. (2015) allows the time-frequency quantification of the amount of surface waves in the total wavefield. The basin effects may then be assessed accurately both in the time as well as in the frequency domain.

6. Acknowledgements

The authors acknowledge the support of ANR project Modulate (brgm.modulate.fr).

7. References

[1] Bard P.Y., Bouchon M. (1985): The two dimensional resonance of sediment filled valleys. *Bulletin of the Seismological Society of America*, **75**, 519-541.

[2] Chaillat S., Bonnet M., Semblat, J.F. (2008): A multi-level Fast Multipole BEM for 3-D elastodynamics in the frequency domain, *Computer Methods and Applied Mechanics and Engineering*, 197, 4233-4249.

[3] Chaillat S., Bonnet M., Semblat J.F. (2009): A new fast multi-domain BEM to model seismic wave propagation and amplification in 3D geological structures, *Geophysical Journal International*, **177**, 509-531.

[4] Chavez-Garcia F.J., Faccioli E. (2000): Complex site effects and building codes: Making the leap, *Journal of Seismology*, **4**, 23-40.

[5] Delépine N., Semblat J.F. (2012): Site effects in an alpine valley with strong velocity gradient: interest and limitations of the 'classical' BEM, *Soil Dynamics and Earthquake Eng.*, **38**, 15-24.

[6] Drawinski M. (2003): Scattering of elastic waves by a general anisotropic basin. Part 2: a 3D model, *Earthquake Engineering and Structural Dynamics*, **32**, 653-670.

[7] Jiang T., Kuribayashi E. (1988): The three-dimensional resonance of axisymmetric sediment-filled valleys, *Soils and Foundations*, **28**(4), 130-146.

[8] Kim J., Papageorgiou A.S. (1993): The Discrete Wavenumber Boundary Element Method for 3D Scattering Problems, *Journal of Engineering Mechanics*, ASCE, **119**(3), 603-624.

[9] Komatitsch D., Vilottte J.P. (1998): The Spectral Element Method: An efficient tool to simulate the seismic response of 2D and 3D geological structures, *Bulletin of the Seismological Society of America*, **88**, 368-392.

[10] Makra K., Chávez-García F.J., Raptakis D., Pitilakis K. (2005): Parametric analysis of the seismic response of a 2D sedimentary valley: Implications for code implementations of complex site effects, *Soil Dynamics & Earthquake Engineering*, **25**, 303-315.

[11] Meza-Fajardo K.C., Varone C., Lenti L., Martino S., Semblat J.F. (2019): Surface wave quantification in a highly heterogeneous alluvial basin: Case study of the Fosso di Vallerano valley, Rome, Italy, *Soil Dynamics and Earthquake Engineering*, **120**, 292-300.

[12] Meza-Fajardo KC, Papageorgiou AS, Semblat JF. (2015): Identification and extraction of surface waves from three-component seismograms based on the Normalized Inner Product, *Bulletin of the Seismological Society of America*, **105**(1), 210-229.

[13] Moczo P., Kristek J., Vavrycuk V., Archuleta R.J., Halada, L. (2002): 3D Heteregeneous Staggered-Grid Finite-Difference Modeling of Seismic Motion with Volume Harmonic and Arithmetic Averaging of Elastic Moduli and Densities, *Bulletin of the Seismological Society of America*, **92**(8), 3042-3066.

[14] Olsen K.B., Nigbor R., Konno T. (2000): 3D viscoelastic wave propagation in the upper Borrego valley, California, constrained by borehole and surface data, *Bulletin of the Seismological Society of America*, **90**(1), 134-150.

[15] Paolucci R., Morstabilini L. (2006): Non-dimensional site amplification functions for basin edge effects of seismic ground motion. *Third International Symposium on the Effects of Surface Geology on Seismic Motion (ESG)*, Grenoble, France.

[16] Rodriguez-Zuñiga J.L., Sanchéz-Sesma F.J., Pérez-Rocha L.E. (1995): Seismic response of shallow alluvial valleys: the use of simplified models, *Bulleting of the Seismological Society of America*, **85**(3), 890-899.

[17] Sánchez-Sesma F.J., Luzón F. (1995): Seismic Response of Three-Dimensional Alluvial Valleys for Incident P, S, and Rayleigh waves, *Bulletin of the Seismological Society of America*, **85**, 269-284.

[18] Smerzini C., Paolucci R., Stupazzini M. (2011): Comparison of 3D, 2D and 1D approaches to predict long period earthquake ground motion in the Gubbio plain, Central Italy, *Bulletin of Earthquake Engineering*, **9**(6), 2007-2029.

[19] Semblat, J. F., M. Kham, E. Parara, P. Y. Bard, K. Pitilakis, K. Makra, D. Raptakis (2005): Site effects: Basin geometry vs soil layering, *Soil Dynamics and Earthquake Eng.*, **25**(7/10), 529 538.

[20] Semblat, J. F., N. Lokmane, L. Driad-Lebeau, and G. Bonnet (2010). Local amplification of deep mining induced vibrations Part 2: Simulation of ground motion in a coal basin, *Soil Dynamics and Earthquake Eng.*, **30**, 947–957.

[21] Yokoi T. (2003): The higher order Born approximation applied to improve the solution of seismic response of a three-dimensional canyon by the Indirect Boundary Method, *Physics of Earth and Planetary Interior*, **137**, 97-106.

